Int J Clin Exp Med 2016;9(2):1190-1199
www.ijcem.com /ISSN:1940-5901/IJCEM0018100

Original Article

Assessment of liver fibrosis: comparison of the liver fibrosis index by real-time ultrasound elastography and the apparent diffusion coefficient by magnetic resonance imaging in a rat model

Genwen Hu[1*], Xing Zhong[2*], Xuhui Zhang[3], Wen Liang[3], Yufa Li[4], Queenie Chan[5], Xianyue Quan[3]

[1]Department of Medical Image Center, Shenzhen Bao'an Maternal and Child Health Hospital, Shenzhen, Guangdong Province, China; [2]Department of Medical Image Center, First Affiliated Hospital, Jinan University, Guangzhou, Guangdong Province, China; [3]Department of Medical Image Center, Zhujiang Hospital, Southern Medical University, Guangzhou, Guangdong Province, China; [4]Department of Pathology, Zhujiang Hospital, Southern Medical University, Guangzhou, Guangdong Province, China; [5]Philips Healthcare, Hong Kong, China. [*]Equal contributors.

Received October 19, 2015; Accepted January 10, 2016; Epub February 15, 2016; Published February 29, 2016

Abstract: Background: non-invasive method, apparent diffusion coefficient (ADC) and the liver fibrosis index (LFI), assessment of liver fibrosis has been one of major objectives in the society of hepatologists. Aim: To explore the variable characteristics of ADC and the LFI in different stages of liver fibrosis in rats and to compare their performance in staging liver fibrosis. Methods: Liver fibrosis model rats (N = 50) were produced by carbon tetrachloride (CCl_4). Surviving model rats (N = 45) and controls (N =15) were subjected to MRI and RTE, and the ADC and LFI values were analyzed. All animals were sacrificed for pathological examination. The liver fibrosis stage (F0-F4) was defined based on the METAVIR score. Nonparametric statistical methods and receiver operating characteristic (ROC) curve analyses were employed to determine diagnostic accuracy. Results: Correlation analysis showed that the liver fibrosis stage was negatively correlated with ADC ($r = -0.732$, $P < 0.001$) and positively correlated with LFI ($r = 0.706$, $P < 0.001$). ROC curves showed that the areas under the curve (AUCs) for ADC and LFI in the prediction of the liver fibrosis stage were 0.781-0.924 and 0.824-0.939, respectively. Conclusions: Both the ADC values and LFI values were strongly correlated with the liver fibrosis stages in our rat model. Moreover, the ADC was sensitive in predicting early-stage liver fibrosis, while the LFI was more accurate in predicting predict intermediate- and late-stage liver fibrosis.

Keywords: Liver fibrosis, magnetic resonance imaging, apparent diffusion coefficient, ultrasound, real-time elastography

Introduction

Liver fibrosis can be induced by chronic viral infections, excessive consumption of alcohol, abnormal metabolism, autoimmune response, and drugs [1, 2]. The consensus is that early-stage liver cirrhosis is reversible [3]. Thus, the early diagnosis of liver fibrosis with a desirable sensitivity and specificity is required for managing these patients.

The traditional imaging-based examinations of liver fibrosis have limited utility [4]. Real-time elastography (RTE) using ultrasound and diffusion-weighted magnetic resonance imaging (DWI) are noninvasive examinations. RTE and DWI have been studied extensively to determine their diagnostic value, often individually. However, few reports have compared both methods in the one and the same study.

DWI can detect the random Brownian motion of water molecules inside human tissues. Measurement of the extent of restriction and the direction of water molecule diffusion can thereby indirectly reflect changes in tissue microstructure. Therefore, DWI is useful in diagnosis of liver fibrosis [5-7]. The apparent diffusion coefficient (ADC) is used to quantify the diffusion coefficient. As reported, the ADC in a

fibrotic liver is lower than the normal level [5-10].

The common B-mode ultrasound is not able to for early detection of liver fibrosis. However, the new technique of RTE has been employed to detect fibrosis in the liver. Differences in the elastic coefficient among tissues can be differentiated by RTE. When the motion amplitude is transformed into real-time color images, the colors of the images reflect the hardness of the tissues. Red usually indicates a soft tissue, while blue indicates a hard one [11, 12]. The cardiovascular beating capacity of the patient is utilized to form a tissue compression image. The liver fibrosis index (LFI), a quantitative parameter, represents the relative severity of fibrosis [13]. The new RTE improves the sensitivity of elastographic signal collection and reduces interference of human factors induced upon measurement.

The purpose of this study was to explore the variable characteristics of ADC and the LFI in different stages of liver fibrosis in rats, and to compare their performance in staging liver fibrosis.

Materials and methods

Experimental animals

Male Sprague-Dawley rats (n = 65, weighing 200 ± 20 g) were provided by the Experimental Animals Center at Southern Medical University (Certificate No. 44002100001642). The rats were housed in cages in an SPF-level environment: 18-20°C, humidity 60-70%; 12-h light and dark cycles. Drinking and eating were not restricted for the rats during the experiment. All experimental animals drank distilled water and were fed with standard rat chow. Animals were regularly monitored, and their general wellbeing was recorded periodically. All experimental procedures were approved by the Institutional Animal Ethics Committee of University.

Modeling method

The 65 rats were randomly divided via a digital meter into the model group (n = 50) or the control group (n = 15). A classical procedure for chemical-induced liver fibrosis was utilized [14, 15]. Briefly, all rats in control group were given magnetic resonance imaging (MRI) examination after 1 week acclimatization. After being acclimatized to the housing conditions for 1 week, 50 rats in liver fibrosis model group were given 50% (v/v) carbon tetrachloride (CCl_4) (0.3 mL/100 g, dissolved in olive oil) by subcutaneous injection. Animals received CCl_4 administration twice weekly for 10 weeks, and the dosage of drug was determined by the animal body weight each time before injection. After the initial injection (Day 0), five rats in model group were randomly selected for MRI examination on Days 14, 21, 28, 35, 42, 49, 56, 63, 70. Animals in model group were sacrificed after MRI examination. A total of 5 rats in model group died during the experiment period.

MRI

Rats were subjected to MRI scan using an Achieva 3.0T TX MRI machine (Philips Healthcare, Best, Netherlands). Rats were prepared for scanning under anesthetization with an intraperitoneal injection of 3% pentobarbital (w/v; 0.2 mL/100 g). Animals were placed in the prone position in a special small animal coil, with their heads positioned straight forward and abdomens secured with a safety belt to reduce respiratory motion. MRI scanning was conducted with standard sequences as follows: (A) axial T2-weighted fast field echo (FFE) images were obtained with time to repetition (TR) of 203 ms, echo time (TE) of 9.2 ms, field of view (FOV) of 60 × 60 mm, imaging matrix of 100 × 100, and slice thickness of 3 mm; (B) axial T1-weighted turbo-spin-echo (TSE) images were obtained with TR of 400 ms, TE of 10 ms, FOV of 60 × 60 mm, imaging matrix of 120 × 93, and slice thickness of 3 mm. For each sequence, 13 slices were obtained.

DWI using the single-shot spin-echo echo-planar imaging sequence was performed. The parameters for DWI scanning were as follows: TR, 2,000 ms; TE, 55 ms; echo-planar imaging factor, 63; FOV, 50 × 50 mm; slice thickness, 3 mm; imaging matrix, 64 × 63; receiver bandwidth, 2,735.7 Hz/pixel; motion probing gradients (MPGs) in three orthogonal axes; *b* values, 0 and 800 s/mm^2; number of signals averaged, 3; parallel imaging (SENSitivity Encoding) factor, 3; and fat suppression, spectral presaturation inversion recovery. A total of 9 representative axial slices through the liver were selected.

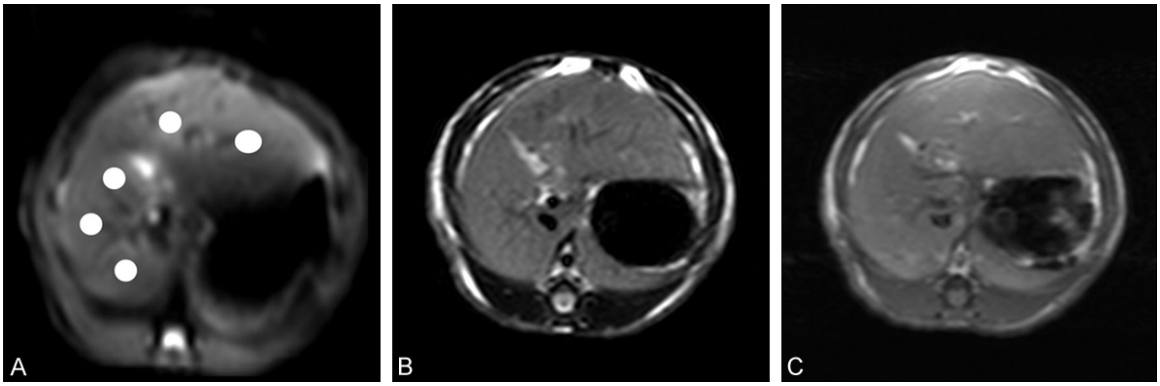

Figure 1. MRI of a rat with stage F2 fibrosis. A. White circles demonstrate regions of interest manually placed on the liver parenchyma with the DWI. B. Axial T2-weighted image. C. Axial T1-weighted image.

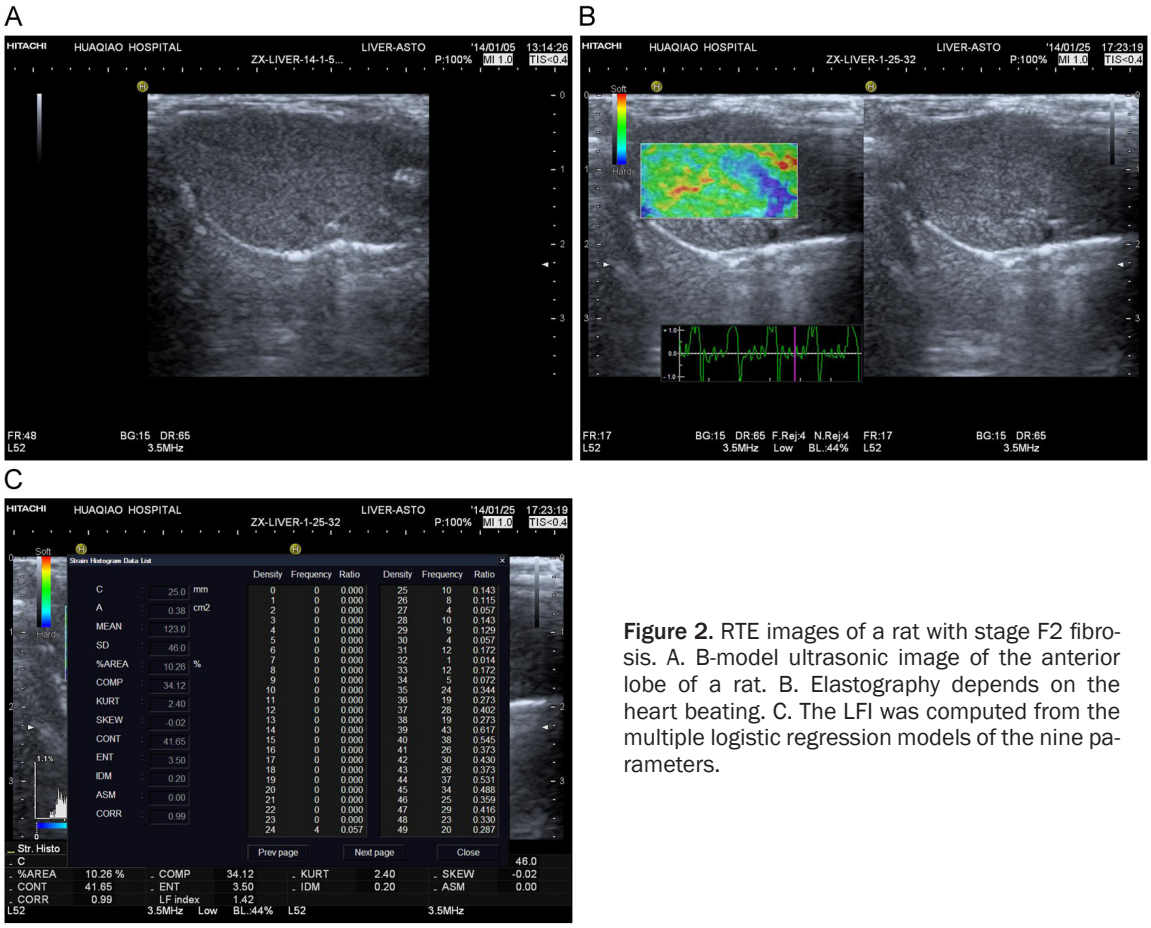

Figure 2. RTE images of a rat with stage F2 fibrosis. A. B-model ultrasonic image of the anterior lobe of a rat. B. Elastography depends on the heart beating. C. The LFI was computed from the multiple logistic regression models of the nine parameters.

Image analysis

The value of ADC was calculated for different *b* values assuming a mono-exponential decay. Images were analyzed using a PRIDE DWI Tool software (version 1.5, Philips Healthcare). Slices of liver parenchyma were screened for selection of the best one. For each sample, 5 regions of interest (ROIs) of approximately 3-4 mm^2 were manually drawn by an experienced radiologist, avoiding the inclusion of bile ducts, vessels or the liver margin. Fits were performed for all ROIs on a pixel-by-pixel basis with the Levenberg-Marquardt algorithm. Subsequent analysis was carried out using Image J software (NIH, Bethesda, MD, USA). The mean values of

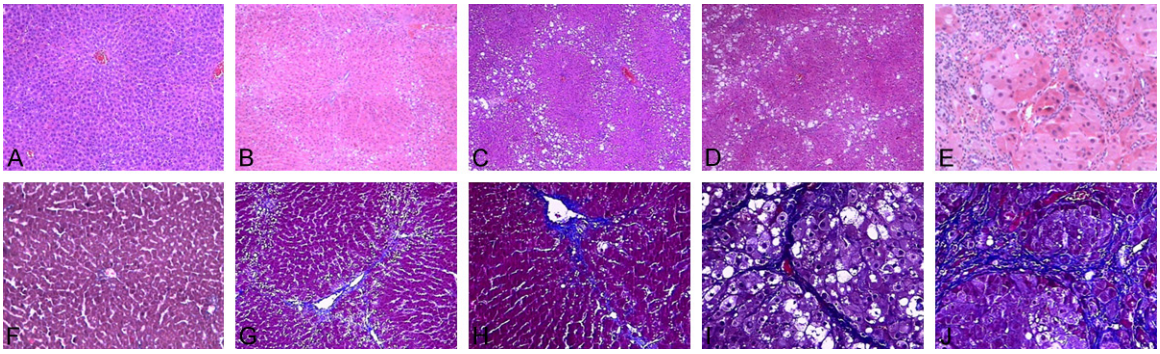

Figure 3. Representative hematoxylin-eosin and Masson's trichrome staining. A-E. Liver fibrosis stages 0-4 (hematoxylin-eosin stain; 10 × 20); F-J. Liver fibrosis stages 0-4 (Masson's stain; 10 × 40).

Table 1. Liver fibrosis index (LFI) and apparent diffusion coefficient (ADC) at different stages of liver fibrosis presented as mean values ± standard deviation (SD) and 95% confidence intervals (CIs); differences between stages were highly significant (P < 0.001)

	n (60)	LFI		ADC (× 10^{-3} mm^2/s)	
		Mean ± SD	CI	Mean ± SD	CI
Fibrosis stage					
0	15	1.22 ± 0.43	0.97-1.45	1.29 ± 0.18	1.19-1.14
1	11	1.53 ± 0.29	1.33-1.72	1.11 ± 0.16	1.00-1.22
2	12	1.61 ± 0.28	1.44-1.79	0.93 ± 0.15	0.84-1.03
3	10	1.95 ± 0.56	1.55-2.35	0.88 ± 0.12	0.79-0.97
4	12	2.53 ± 0.61	2.26-2.78	0.87 ± 0.10	0.82-0.93
P value		< 0.001		< 0.001	

selected ROIs (n = 5) were calculated (**Figure 1**).

Ultrasonic examination

Ultrasonic imaging (Hitachi HI Vision Preirus ultrasound meter, Hitachi Medical, Tokyo, Japan) was immediately performed after MRI scanning. A linear array probe at a frequency 5-13 MHz (central frequency of 8 MHz) was used. The rats were fixed in the dorsal position and underwent liver examination. Double amplitudes were simultaneously displayed as an elastic image on the left side and a 2D image on the right side. The elastography depends on the heart beating. Along with the heart contraction and diastole, the lower left part of the motion meter's screen displays the liver compression curves (stress strain curve), which represent the compression tensile modulus and the impact frequency produced by the liver tissues under heart beating. If the stress strain curve shows five or more continuous stable waveforms, the image is frozen. Next, the built-in data processing system was transferred to measure the LFI within a ROI. Each rat was examined 10 times, and the mean value was computed.

The ROI was set at the anterior lobe, but attention was paid to avoid blood vessels, bile ducts, and liver margins. The strain value in the ROI was represented by colors from 0 (red) to 255 (blue), indicating a hardness range from absent to complete. In addition, histograms and nine parameters were generated, including the mean of the relative strain value (MEAN), ratio of the blue area in the analyzed region (% AREA), standard deviation of the relative strain value (SD), complexity of the blue area (COMP), skewness of the strain histogram (SKEW), kurtosis of the strain histogram (KURT), inverse difference moment (IDM), entropy (ENT), and angular second moment (ASM).

LFI was computed from the multiple logistic regression models of the above nine parameters [13, 16] as follows: LFI = (-0.00897 × MEAN) - (0.00502 × SD) + (0.00232 × % AREA) + (0.0253 × COMP) + (0.775 × SKEW) - (0.281 × KURT) + (2.08 × ENT) + (3.04 × IDM) + (40.0 × ASM) - 5.54 (**Figure 2**).

Histopathology

All rats were sacrificed by intraperitoneal injection of an overdose of 3% pentobarbital at various time points after MRI scanning and ultrasonic detection (5-15 h). Livers were fixed in 10% formalin. The sections were stained with

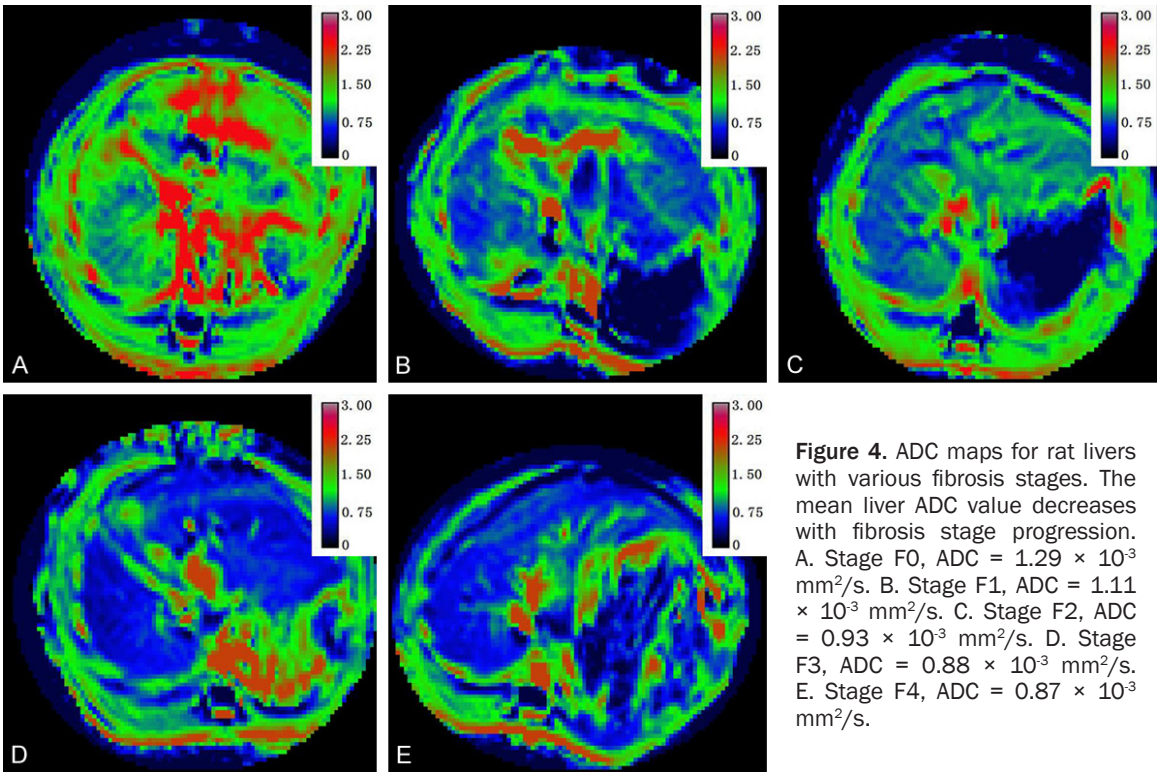

Figure 4. ADC maps for rat livers with various fibrosis stages. The mean liver ADC value decreases with fibrosis stage progression. A. Stage F0, ADC = 1.29 × 10^{-3} mm^2/s. B. Stage F1, ADC = 1.11 × 10^{-3} mm^2/s. C. Stage F2, ADC = 0.93 × 10^{-3} mm^2/s. D. Stage F3, ADC = 0.88 × 10^{-3} mm^2/s. E. Stage F4, ADC = 0.87 × 10^{-3} mm^2/s.

hematoxylin & eosin and Masson's for histology, and photographed with Leica DM2000.

Liver fibrosis stages were scored by author LYF (an experienced histopathologist with 9 years of liver pathology experience) using the METAVIR classification system [17], with the following stage definitions: F0 = no fibrosis; F1 = portal fibrosis without septa; F2 = portal fibrosis and a few septa; F3 = numerous septa without cirrhosis; and F4 = cirrhosis.

Statistical analysis

Statistical analysis was performed by one-way analysis of variance (ANOVA) for multiple group comparisons of the parameters using SPSS 20.0. Spearman's rank correlation coefficients, *r* values, were calculated to assess the correlation. Receiver operating characteristic (ROC) curves and the area under the ROC curve (AUC) were used to evaluate the usefulness of parameters for predicting the fibrosis stage. A *P*-value ≤ 0.05 was considered statistically significant.

Results

Pathological results

Five rats in the model group died during the process of intervention, and the remaining 45 rats were pathologically scored for liver fibrosis: F1 = 11, F2 = 12, F3 = 10, and F4 = 12. All rats in the control group completed the experimental analysis (F0 = 15) (**Figuire 3**).

ADC and LBI scores in different stages of liver fibrosis

Our results showed that the ADC declined while the LFI increased along with the progression of fibrosis (**Table 1**; **Figures 4** and **5**). Both the ADC and LFI in all groups were analyzed by ANOVA. Both indices were significantly different among the five groups ($P < 0.001$).

Correlation analysis showed that the ADC was negatively correlated with the liver fibrosis stage ($r = -0.732$, $P < 0.001$, CI: -0.826--0.582), but the LFI was positively correlated with the progression of fibrosis ($r = 0.706$, $P < 0.001$, CI: 0.525-0.831).

ROC curve analysis

ROC curve analysis showed that ADC and LFI predicted the liver fibrosis stage with high sensitivity and specificity. At the early stages (F0 vs. F1-F4, F0-F1 vs. F2-F4), the area under curve (AUC) of ADC was larger than that of LFI, but at intermediate and late stages (F0-F2 vs.

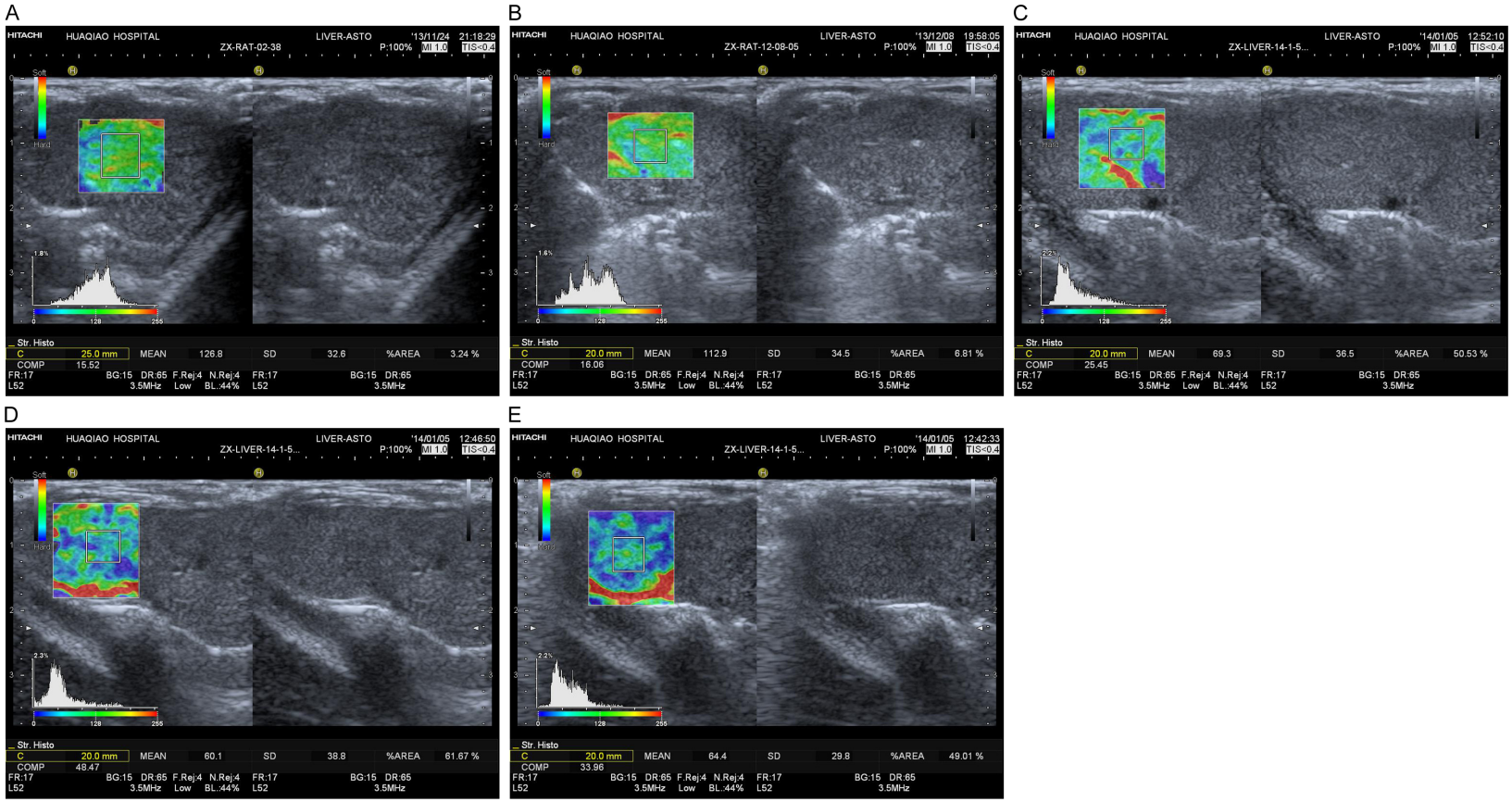

Figure 5. RTE maps for rat livers with different fibrosis stages. The mean LFI values increase with fibrosis stage progression: (A) Stage F0, LFI = 1.22; (B) Stage F1, LFI = 1.53; (C) Stage F2, LFI = 1.61; (D) Stage F3, LFI = 1.95; and (E) Stage F4, LFI = 2.53.

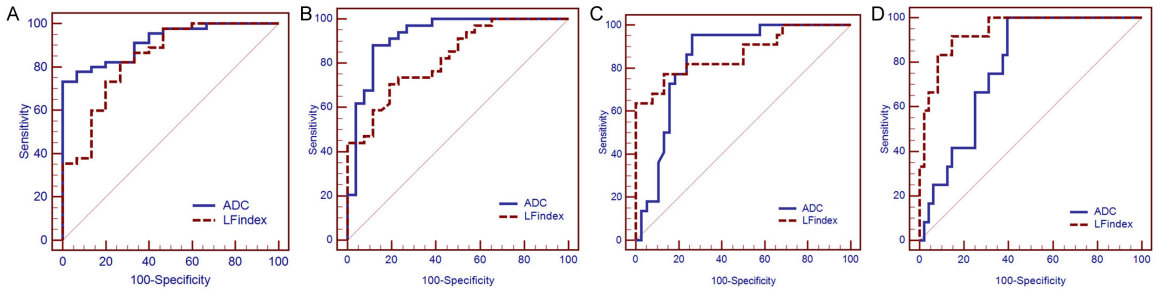

Figure 6. ROC curves of ADC and LFI for differentiation of fibrosis stages. A. F0 vs. F1-F4, area under ROC curve (AUC): ADC = 0.917, LFI = 0.840. B. F0–F1 vs. F2–F4, AUC: ADC = 0.924, LFI = 0.824. C. F0-F2 vs. F3-F4, AUC: ADC = 0.842, LFI = 0.867. D. F0-F3 vs. F4, AUC: ADC = 0.781, LFI = 0.939.

Table 2. Performance of the selected apparent diffusion coefficient (ADC) and liver fibrosis index (LFI) cut-off values in predicting METAVIR fibrosis stages

Parameter, *comparison*		Cut-off value	Sensitivity	95% CI	Specificity	95% CI	+LR	-LR
ADC	*F0 vs. F1-4*	≤ 1.10	80.00	65.4-90.4	86.67	59.5-98.3	6.00	0.23
	F0-1 vs. F2-4	≤ 1.04	88.24	72.5-96.7	88.46	69.8-97.6	7.65	0.13
	F0-2 vs. F3-4	≤ 1.01	95.45	77.2-99.9	73.68	56.9-86.6	3.63	0.06
	F0-3 vs. F4	≤ 0.98	83.33	51.6-97.9	62.50	47.4-76.0	2.22	0.27
LFI	*F0 vs. F1–4*	> 1.37	82.22	67.9-92.0	73.33	44.9-92.2	3.08	0.24
	F0-1 vs. F2-4	> 1.64	70.59	52.5-84.9	80.77	60.6-93.4	3.67	0.36
	F0-2 vs. F3-4	> 1.82	77.27	54.6-92.2	86.84	71.9-95.6	5.87	0.26
	F0-3 vs. F4	> 1.98	91.67	61.5-99.8	85.42	72.2-93.9	6.29	0.10

F3-F4, F0-F3 vs. F4), the AUC of LFI was larger than that of ADC (**Figure 6**). The sensitivity and specificity under the optimal cutoff of each pathological stage that were predicted using Youden's index are listed in **Table 2**.

Discussion

In conclusion, Current clinical diagnostic methods for detecting liver fibrosis include liver biopsy, serology, and imaging. Liver biopsy-based histology presents direct evidence of liver fibrosis. However, the procedure is invasive and sampling errors [18, 19]. Furthermore, biopsies are difficult to obtain for dynamic observation [20]. Serology also has serious limitations in terms of sensitivity and specificity [21, 22]. Meanwhile, traditional imaging methods have a low specificity. RTE by ultrasound and DWI are noninvasive methods that have advantages over traditional methods. However, RTE and DWI are different in imaging mechanisms with pathophysiology.

To investigate the diagnostic value of the ADC and LFI at differentiating liver fibrosis stages, in this study, we measured both the ADC by MRI and the LFI by ultrasound in rats with experimentally induced fibrosis that was histologically graded. We found that both the ADC and LFI were strongly correlated with the progression of liver fibrosis. ROC curve analysis showed that both the ADC and LFI were highly sensitive and specific at predicting the liver fibrosis stage.

A declining ADC value during the formation of liver fibrosis and cirrhosis has been well recognized [6, 23]. Most scholars agree that the decreased ADC values primarily arise from the changing properties of a fibrotic liver, which include diffused hyperplasia of abundant fibrous tissues in the extracellular space, degenerative edema in hepatocytes, and inflammation in both the portal region and parenchyma. All of these changes increase resistance to the dispersion of water molecules [5-7]. In addition, the reduction of ADC may be attributed to the alteration of liver microcirculation [8-10]. Changes in intrahepatic fats and iron contents also can impact the ADC [24].

The fibrosis stage was inversely correlated with the ADC ($r = -0.732$, $P < 0.001$). This correlation

is higher than those reported previously between ADC values and fibrosis stage, which are r = -0.654, P = 0.001 [25]; r = -0.54, P < 0.0001 [26], and r = -0.41 [27].

The value of ADC in assessment of liver fibrosis staging is still a subject of scientific debate. Some researchers found that the ADC does not accurately determine the stage [6, 24, 28]. Others have suggested that the ADC does accurately evaluate the degree of liver fibrosis [26, 29, 30]. In this study, the ADC revealed a good predictive value for diagnosing the stage of liver fibrosis (AUC: 0.781-0.924), which is consistent with results of Fujimoto *et al*. [30] (AUC: 0.842-0.926) and Bonekamp *et al*. [26] (AUC: 0.77-0.79).

We also noted that the AUC of ADC staging early-stage was larger than that at late stage. Liver cell swelling and fat solubilization were alleviated at stages F3-F4. On the other hand, the deposition of EMC was gradually intensified. Thus, the uncertain ADC values in fibrosis stage F2 to stage F4 [31].

RTE is a novel ultrasonic technique for detecting liver fibrosis. The diffuse hyperplasia of abundant fibrous tissues in the extracellular space increases the liver hardness during the fibrotic process. The changing composition of the hepatic parenchyma can be displayed by RTE. The basic principle of elastography is that changes in echo signal migration amplitudes before and after compression are transformed into real-time color images as follows: an echo in the tissues with a small elastic coefficient will move longer after compression and is displayed as red; an echo that travels a shorter distance in tissues with a large elastic coefficient is displayed as blue; and an echo that travels an intermediate distance in tissues with a medium elastic coefficient is displayed as green. Thus, the tissue hardness is reflected by different colors. The LFI, computed from multiple logistic regression models, suggests the extent of fibrosis in a quantitative manner.

Despite the article points out that the LFI is evaluation of HCV usually [32], but studies showed that LFI useful in liver fibrosis caused by variety of reasons [33-35].

Many studies have used RTE to determine the liver fibrosis stage. High accuracies with AUC values of 0.66-0.93, 0.87-0.88, 0.87-0.91, and 0.91-0.94 have been reported [36-39] in the staging of liver fibrosis through ROC curve analyses.

In this study, the LFI showed a high accuracy (AUC: 0.824-0.939) in the prediction of liver fibrosis. The LFI was positively correlated with the degree of liver fibrosis (r = 0.706), which signaled that liver tissue was gradually hardened along with the repair process, demonstrating a fundamental change in the fibrotic liver.

At early stages of fibrosis (F0 vs. F1-F4, F0-F1 vs. F2-F4), the AUC of the ADC was larger; thus, because the sedimentation of collagen fibers was not the main pathological change at the early stages. So the hardness of liver parenchyma is not obvious. However, once the fibrosis was at an intermediate or late stage, the AUC of LFI was larger than that of ADC. The deposition of collagen fibers accumulated, resulting in significantly increased liver hardness and an increased LFI value.

Limitations of our study: This study was based on a rat fibrosis model, and the findings may not be fully applicable to human liver fibrosis. However, the diagnostic utility of staging fibrosis by both the ADC and LFI seems promising and is worthy of further investigation in the clinic.

In conclusion, In spite of different imaging mechanisms by RTE and DWI, both the ADC as determined by MRI and the LFI as determined by RTE were strongly correlated with liver fibrosis progression. Moreover, the ADC was more sensitive in predicting early-stage liver fibrosis, while the LFI was more accurate predicting intermediate- and late-stage liver fibrosis. Our results suggest that both RTE and DWI should be utilized in staging fibrosis and a combination of two measurements will increase the staging accuracy.

Acknowledgements

This study was supported by grant from the Guangdong Province Natural Science Foundation (grant no. 2015A030313269). The funders had no role in study design, data collection and analysis, decision to publish, or preparation of the manuscript. And the work was not funded by any industry sponsors.

Disclosure of conflict of interest

None.

Address correspondence to: Xianyue Quan, Department of Medical Image Center, Zhujiang Hospital, Southern Medical University, Guangzhou 510282, Guangdong Province, China. Tel: 020-61643460; Fax: 020-61643460; E-mail: quanxianyue2014@163.com

References

[1] Malekzadeh R, Mohamadnejad M, Nasseri-Moghaddam S, Rakhshani N, Tavangar SM, Sohrabpour AA and Tahaghoghi S. Reversibility of cirrhosis in autoimmune hepatitis. Am J Med 2004; 117: 125-129.

[2] Schuppan D and Afdhal NH. Liver cirrhosis. Lancet 2008; 371: 838-851.

[3] Marcellin P, Gane E, Buti M, Afdhal N, Sievert W, Jacobson IM, Washington MK, Germanidis G, Flaherty JF, Schall RA, Bornstein JD, Kitrinos KM, Subramanian GM, McHutchison JG and Heathcote EJ. Regression of cirrhosis during treatment with tenofovir disoproxil fumarate for chronic hepatitis B: a 5-year open-label follow-up study. Lancet 2013; 381: 468-475.

[4] Wang YX and Yuan J. Evaluation of liver fibrosis with T1rho MR imaging. Quant Imaging Med Surg 2014; 4: 152-155.

[5] Sandrasegaran K, Akisik FM, Lin C, Tahir B, Rajan J, Saxena R and Aisen AM. Value of diffusion-weighted MRI for assessing liver fibrosis and cirrhosis. AJR Am J Roentgenol 2009; 193: 1556-1560.

[6] Koinuma M, Ohashi I, Hanafusa K and Shibuya H. Apparent diffusion coefficient measurements with diffusion-weighted magnetic resonance imaging for evaluation of hepatic fibrosis. J Magn Reson Imaging 2005; 22: 80-85.

[7] Lewin M, Poujol-Robert A, Boelle PY, Wendum D, Lasnier E, Viallon M, Guechot J, Hoeffel C, Arrive L, Tubiana JM and Poupon R. Diffusion-weighted magnetic resonance imaging for the assessment of fibrosis in chronic hepatitis C. Hepatology 2007; 46: 658-665.

[8] Luciani A, Vignaud A, Cavet M, Tran Van Nhieu J, Mallat A, Ruel L, Laurent A, Deux JF, Brugieres P and Rahmouni A. Liver cirrhosis: intravoxel incoherent motion MR imaging-Pilot study 1. Radiology 2008; 249: 891-899.

[9] Annet L, Peeters F, Abarca-Quinones J, Leclercq I, Moulin P and Van Beers BE. Assessment of diffusion-weighted MR imaging in liver fibrosis. J Magn Reson Imaging 2007; 25: 122-128.

[10] Girometti R, Furlan A, Esposito G, Bazzocchi M, Como G, Soldano F, Isola M, Toniutto P and Zuiani C. Relevance of b-values in evaluating liver fibrosis: A study in healthy and cirrhotic subjects using two single-shot spin-echo echo-planar diffusion-weighted sequences. J Magn Reson Imaging 2008; 28: 411-419.

[11] Obara N, Ueno Y, Fukushima K, Nakagome Y, Kakazu E, Kimura O, Wakui Y, Kido O, Ninomiya M and Kogure T. Transient elastography for measurement of liver stiffness measurement can detect early significant hepatic fibrosis in Japanese patients with viral and nonviral liver diseases. J Gastroenterol 2008; 43: 720-728.

[12] Kanamoto M, Shimada M, Ikegami T, Uchiyama H, Imura S, Morine Y, Kanemura H, Arakawa Y and Nii A. Real time elastography for noninvasive diagnosis of liver fibrosis. J Hepatobiliary Pancreat Surg 2009; 16: 463-467.

[13] Tomeno W, Yoneda M, Imajo K, Suzuki K, Ogawa Y, Shinohara Y, Mawatari H, Fujita K, Shibata W and Kirikoshi H. Evaluation of the Liver Fibrosis Index calculated by using real-time tissue elastography for the non-invasive assessment of liver fibrosis in chronic liver diseases. Hepatol Res 2013; 43: 735-742.

[14] Zhang Y, Ikegami T, Honda A, Miyazaki T, Bouscarel B, Rojkind M, Hyodo I and Matsuzaki Y. Involvement of integrin-linked kinase in carbon tetrachloride-induced hepatic fibrosis in rats. Hepatology 2006; 44: 612-622.

[15] Wu F, Huang S, Zhu N, Liu W, Zhang Y and He Y. Recombinant human histidine triad nucleotide-binding protein 1 attenuates liver fibrosis induced by carbon tetrachloride in rats. Mol Med Rep 2013; 8: 1023-1028.

[16] Tatsumi C, Kudo M, Ueshima K, Kitai S, Ishikawa E, Yada N, Hagiwara S, Inoue T, Minami Y, Chung H, Maekawa K, Fujimoto K, Kato M, Tonomura A, Mitake T and Shiina T. Non-invasive evaluation of hepatic fibrosis for type C chronic hepatitis. Intervirology 2010; 53: 76-81.

[17] Poynard T, Bedossa P and Opolon P. Natural history of liver fibrosis progression in patients with chronic hepatitis C. The OBSVIRC, METAVIR, CLINIVIR, and DOSVIRC groups. Lancet 1997; 349: 825-832.

[18] Vuppalanchi R, Unalp A, Van Natta ML, Cummings OW, Sandrasegaran KE, Hameed T, Tonascia J and Chalasani N. Effects of liver biopsy sample length and number of readings on sampling variability in nonalcoholic Fatty liver disease. Clin Gastroenterol Hepatol 2009; 7: 481-486.

[19] Yoshioka K and Hashimoto S. Can non-invasive assessment of liver fibrosis replace liver biopsy? Hepatol Res 2012; 42: 233-240.

[20] Thampanitchawong P and Piratvisuth T. Liver biopsy: complications and risk factors. World J Gastroenterol 1999; 5: 301-304.

[21] Bissell DM. Assessing fibrosis without a liver biopsy: are we there yet? Gastroenterology 2004; 127: 1847-1849.
[22] Tsukamoto T, Yamamoto T, Ikebe T, Takemura S, Shuto T, Kubo S, Hirohashi K and Kinoshita H. Serum markers of liver fibrosis and histologic severity of fibrosis in resected liver. Hepatogastroenterology 2004; 51: 777-780.
[23] Girometti R, Furlan A, Bazzocchi M, Soldano F, Isola M, Toniutto P, Bitetto D and Zuiani C. Diffusion-weighted MRI in evaluating liver fibrosis: a feasibility study in cirrhotic patients. Radiol Med 2007; 112: 394-408.
[24] Bülow R, Mensel B, Meffert P, Hernando D, Evert M and Kühn JP. Diffusion-weighted magnetic resonance imaging for staging liver fibrosis is less reliable in the presence of fat and iron. Eur Radiol 2013; 23: 1281-1287.
[25] Taouli B, Tolia AJ, Losada M, Babb JS, Chan ES, Bannan MA and Tobias H. Diffusion-weighted MRI for quantification of liver fibrosis: preliminary experience. AJR Am J Roentgenol 2007; 189: 799-806.
[26] Bonekamp S, Torbenson MS and Kamel IR. Diffusion-weighted magnetic resonance imaging for the staging of liver fibrosis. J Clin Gastroenterol 2011; 45: 885-892.
[27] Yoon JH, Lee JM, Baek JH, Shin CI, Kiefer B, Han JK and Choi BI. Evaluation of Hepatic Fibrosis Using Intravoxel Incoherent Motion in Diffusion-Weighted Liver MRI. J Comput Assist Tomogr 2014; 38: 110-116.
[28] Boulanger Y, Amara M, Lepanto L, Beaudoin G, Nguyen BN, Allaire G, Poliquin M and Nicolet V. Diffusion-weighted MR imaging of the liver of hepatitis C patients. NMR Biomed 2003; 16: 132-136.
[29] Do RK, Chandanara H, Felker E, Hajdu CH, Babb JS, Kim D and Taouli B. Diagnosis of liver fibrosis and cirrhosis with diffusion-weighted imaging: value of normalized apparent diffusion coefficient using the spleen as reference organ. AJR Am J Roentgenol 2010; 195: 671-676.
[30] Fujimoto K, Tonan T, Azuma S, Kage M, Nakashima O, Johkoh T, Hayabuchi N, Okuda K, Kawaguchi T, Sata M and Qayyum A. Evaluation of the mean and entropy of apparent diffusion coefficient values in chronic hepatitis C: correlation with pathologic fibrosis stage and inflammatory activity grade. Radiology 2011; 258: 739-748.
[31] Hu G, Chan Q, Quan X, Zhang X, Li Y, Zhong X and Lin X. Intravoxel incoherent motion MRI evaluation for the staging of liver fibrosis in a rat model. J Magn Reson Imaging 2015; 42: 331-9.
[32] Tamaki N, Kurosaki M, Matsuda S, Nakata T, Muraoka M, Suzuki Y, Yasui Y, Suzuki S, Hosokawa T, Nishimura T, Ueda K, Tsuchiya K, Nakanishi H, Itakura J, Takahashi Y, Matsunaga K, Taki K, Asahina Y and Izumi N. Prospective comparison of real-time tissue elastography and serum fibrosis markers for the estimation of liver fibrosis in chronic hepatitis C patients. Hepatol Res 2014; 44: 720-727.
[33] Shi Y, Wang XH, Zhang HH, Zhang HQ, Tu JZ, Wei K, Li J and Liu XL. Quantitative analysis of real-time tissue elastography for evaluation of liver fibrosis. Int J Clin Exp Med 2014; 7: 1014-1021.
[34] Yada N, Kudo M, Morikawa H, Fujimoto K, Kato M and Kawada N. Assessment of liver fibrosis with real-time tissue elastography in chronic viral hepatitis. Oncology 2013; 84 Suppl 1: 13-20.
[35] Lin SH, Ding H, Mao F, Xue LY, Lv WW, Zhu HG, Huang BJ and Wang WP. Non-invasive assessment of liver fibrosis in a rat model: shear wave elasticity imaging versus real-time elastography. Ultrasound Med Biol 2013; 39: 1215-1222.
[36] Hu Q, Zhu S, Kang L, Wang X, Lun H and Xu C. Non-invasive assessment of liver fibrosis using real-time tissue elastography in patients with chronic hepatitis B. Clin Radiol 2014; 69: 194-199.
[37] Wang J, Guo L, Shi X, Pan W, Bai Y and Ai H. Real-time elastography with a novel quantitative technology for assessment of liver fibrosis in chronic hepatitis B. Eur J Radiol 2012; 81: e31-36.
[38] Friedrich-Rust M, Ong MF, Herrmann E, Dries V, Samaras P, Zeuzem S and Sarrazin C. Real-time elastography for noninvasive assessment of liver fibrosis in chronic viral hepatitis. AJR Am J Roentgenol 2007; 188: 758-764.
[39] Morikawa H, Fukuda K, Kobayashi S, Fujii H, Iwai S, Enomoto M, Tamori A, Sakaguchi H and Kawada N. Real-time tissue elastography as a tool for the noninvasive assessment of liver stiffness in patients with chronic hepatitis C. J Gastroenterol 2011; 46: 350-358.